NMR investigation of the diluted magnetic semiconductor Li(Zn_{1−x}Mn_{x})P (x=0.1)

Cui Ding, Chuan Qin, Huiyuan Man, T. Imai, and F. L. Ning

Phys. Rev. B **88**, 041108 — Published 31 July 2013

DOI: 10.1103/PhysRevB.88.041108

NMR Investigation of the Diluted Magnetic Semiconductor Li($Zn_{1-x}Mn_x$)P (x = 0.1)

Cui Ding[1], Chuan Qin[1], Huiyuan Man[1], T. Imai[2,3] and F.L. Ning[1,*]
[1]*Department of Physics, Zhejiang University, Hangzhou 310027, China*
[2]*Department of Physics and Astronomy, McMaster University, Hamilton, Ontario L8S4M1, Canada and*
[3]*Canadian Institute for Advanced Research, Toronto, Ontario M5G1Z8, Canada*
(Dated: July 23, 2013)

We employ NMR techniques to investigate the nature of Mn spins in the I-II-V diluted magnetic semiconductor Li($Zn_{1-x}Mn_x$)P (x = 0.1, Curie temperature T_c = 25 K). We successfully identify the ^{7}Li NMR signals arising from the Li sites adjacent to Mn^{2+}, and probe the static and dynamic properties of Mn spins. From the NMR spin-lattice relaxation data, we show that the Mn spin-spin interactions extend over many unit cells.

PACS numbers: 75.50.Pp, 76.60.-k

The successful fabrication of ($Ga_{1-x}Mn_x$)As ferromagnetic thin films by molecular beam epitaxy (MBE) techniques[1] generated great interest in the research into diluted magnetic semiconductors (DMS)[2–4]. The quality of the epitaxial films steadily improved, and the Curie temperature, T_c, has reached as high as 190 K at the doping level of x = 12 %[5]. The spintronic applications of the DMS may soon become a reality once the T_c exceeds room temperature[6]. Nonetheless, understanding the physical properties of the DMS remains a major challenge[7,8]. A fundamental difficulty stems from the fact that the synthesis of the bulk form of ($Ga_{1-x}Mn_x$)As is impossible beyond the very low solubility limit of $x \sim$ 1%, excluding the possibilities to employ typical microscopic probes of magnetism, such as NMR and neutron scattering techniques.

Recently, Deng et al. reported the successful synthesis of a bulk Li($Zn_{1-x}Mn_x$)As DMS with T_c as high as $\sim$ 50 K based on the I-II-V direct-gap semiconductor LiZnAs[9]. The structure of LiZnAs, shown in Fig. 1(a), can be viewed as an analogue of GaAs with the Zinc-blende structure, see Fig. 1(b); notice that if we replace Ga^{3+} sites of GaAs with Zn^{2+} and place Li^+ ions between Zn^{2+}, we obtain LiZnAs. Also notice that the total number of electrons in $(ZnAs)^-$ is equal to that of GaAs. LiZnAs has a direct band gap of $\sim$ 1.6 eV[12–15], which is comparable to that of GaAs (1.42 eV). On the other hand, the isovalent substitution of Mn^{2+} for Zn^{2+} resembles that of II-VI DMS, although it is difficult to control the carrier density in the latter[10,11]. Recent μSR measurements of Li($Zn_{1-x}Mn_x$)As[9] have established that the magnetically ordered volume reaches 100 % below T_c, and the magnitudes of the ferromagnetic exchange coupling and the ordered moment are comparable to those of (Ga,Mn)As[16]. More recently, some of us[17] found that the iso-structural direct-gap semiconductor LiZnP[12,18] also undergoes a ferromagnetic transition upon Mn doping, and its bulk magnetic properties are very similar to those of LiZnAs.

In this paper, we use ^{7}Li NMR to investigate $LiZn_{0.9}Mn_{0.1}P$ (T_c = 25 K). Since NMR probes the electronic properties in the immediate vicinity of the observed nuclear spins, our NMR measurements will provide *local* and *site-selective* information for $LiZn_{0.9}Mn_{0.1}P$. In this context, it is worth recalling that NMR measurements provided vital microscopic information on the nature of dilute magnetic spins doped into, e.g. simple metals[19] and high T_c superconductors[20]. By successfully identifying ^{7}Li NMR signals arising from the nearest-neighbor (n. n.) Li site of doped Mn (denoted

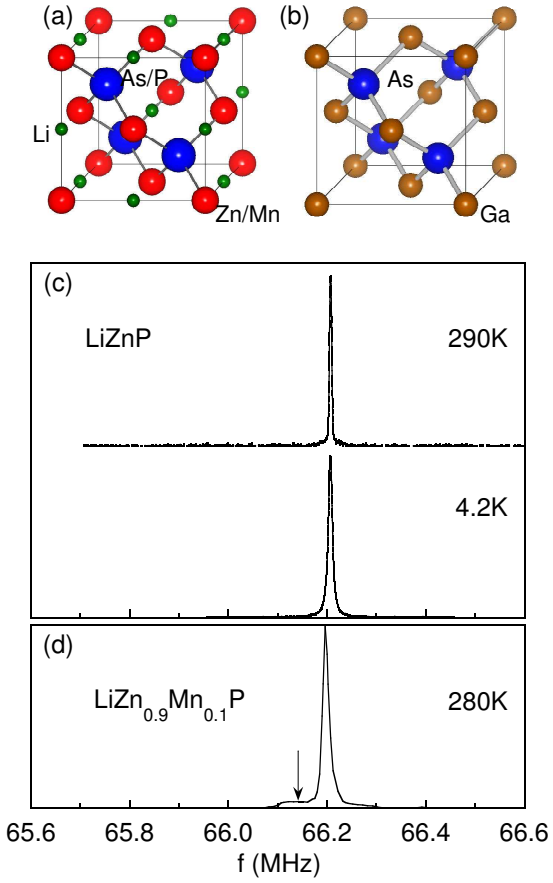

FIG. 1: (Color online) The crystal structure of (a) LiZnP, and (b) GaAs. The representative ^{7}Li lineshapes in 4 Tesla of (c) the parent compound LiZnP, and (d) $LiZn_{0.9}Mn_{0.1}P$. The vertical arrow marks Li(Mn), the n. n. site of doped Mn.

as the Li(Mn) site hereafter), we were able to probe the static and dynamic properties of Mn magnetic moments using NMR in the paramagnetic state of DMS for the first time.

The polycrystalline LiZnP and $LiZn_{0.9}Mn_{0.1}P$ were synthesized by the solid state reaction method. High purity elements of Li (99.9%), Zn (99.9%), Mn (99.99%), and P (99%) were mixed and slowly heated to 450°C in evacuated silica tubes, and held for 48 hours before cooling down to room temperature at the rate of 20°C/h. X-ray diffraction showed that both specimens are single phase with a cubic structure. The lattice constants are 5.7371 Å and 5.7434 Å for LiZnP and $LiZn_{0.9}Mn_{0.1}P$, respectively. We also confirmed from the *dc*-magnetization and μSR measurements that the ferromagnetic ordering is of bulk nature with $T_c = 25$ K. The Hall effect measurements conducted for samples prepared under the identical conditions showed that $LiZn_{0.9}Mn_{0.1}P$ is a hole-doped semiconductor with a very low carrier concentration of $p \sim 3 \times 10^{17}$ cm^{-3}[17]. We will report the complete details of synthesis and characterization of the $LiZn_{0.9}Mn_{0.1}P$ sample by X-ray diffraction, electrical resistance, and μSR elsewhere[17].

We show representative ^{7}Li NMR lineshapes of the parent compound LiZnP in Fig. 1 (c). ^{7}Li has nuclear spin $I = \frac{3}{2}$, and the gyromagnetic ratio is $^7\gamma_n/2\pi = 16.546$ MHz/Tesla. In the external magnetic field $B_{ext} = 4$ Tesla, resonance would take place at $f_0 = (^7\gamma_n/2\pi)B_{ext}$ = 66.184 MHz in the absence of hyperfine interactions with electrons. In general, three NMR peaks for the I_z = m to m+1 transition (m = $-\frac{3}{2}$, $-\frac{1}{2}$, $\frac{1}{2}$) could arise for each inequivalent Li site, if there exists significant interaction between the nuclear quardrupole moment and the electric field gradient (EFG). For the parent compound LiZnP only one Li peak is observed at f_0 $\sim$ 66.206 MHz, as shown in Fig. 1(c). This is because Li atoms are located in a nearly cubic environment, and the EFG is extremely small due to the high symmetry of the lattice. The half height full width (HHFW) of this peak is $\sim$ 5 KHz at 290 K, indicating the high quality of the polycrystalline sample. The very small NMR Knight shift (a.k.a. the paramagnetic frequency shift)[21], $^7K = (66.206 - 66.184)/66.184 = 0.0003$ (i.e. +0.03 %, or +300 ppm), is consistent with the absence of conduction electrons or magnetic moments.

The substitution of Mn drastically alters the ^{7}Li NMR lineshape of $LiZn_{0.9}Mn_{0.1}P$ as shown in Fig. 1(d). To enhance the extra features, we plot the temperature dependence of ^{7}Li NMR lineshapes in a semi-logarithmic scale in Fig. 2. In addition to the relatively sharp but somewhat asymmetrical Li(0) peak that corresponds to the single peak of LiZnP, a broad hump appears on the lower frequency side, as marked by a downward arrow in Fig. 1(d) and the shadowed area in Fig. 2. This broad hump should be attributed to Li(Mn) sites whose magnetic environment is altered by the substitution of the Zn^{2+} sites in their vicinity by Mn^{2+} ions. Upon decreasing the temperature from 280 K to 30 K, the Li(Mn) peak shifts progressively towards lower frequencies, and becomes as broad as 3 MHz. These striking featues of the Li(Mn) peak should be attributed to the spin polarization transferred from the n. n. Mn sites through weak but finite hybridizations between Mn 3*d* and Li orbitals. We define the NMR Knight shift of the Li(Mn) sites at the center of the broad hump, as marked by downward arrows in Fig. 2. We summarize the temperature dependence of $-^7K$ measured in $B_{ext} = 4$ T for the Li(Mn) sites in Fig. 3. $-^7K$ exhibits identical temperature dependence to the bulk magnetization M as measured by

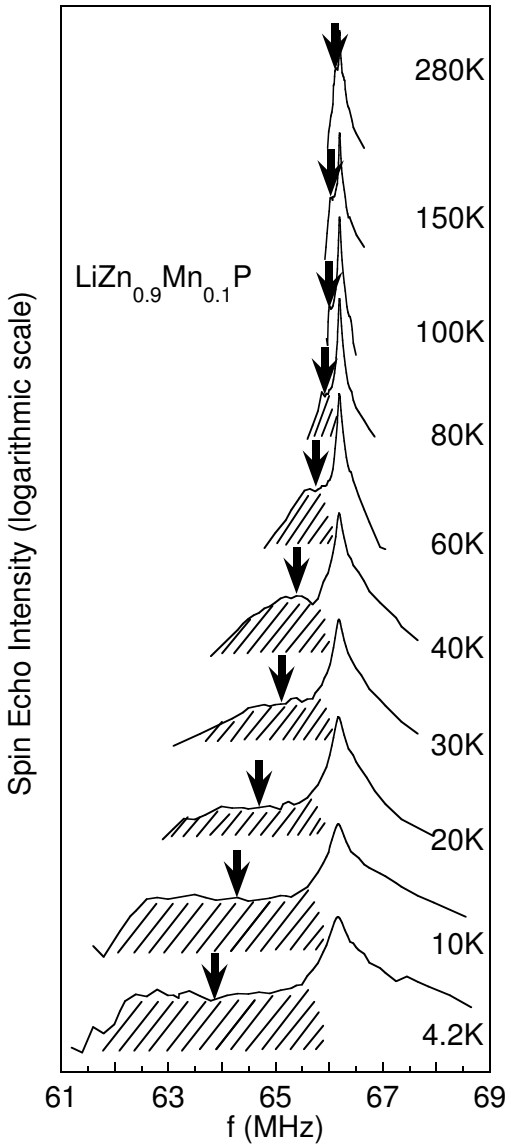

FIG. 2: The temperature dependence of the ^{7}Li NMR line of $Li(Zn_{0.9}Mn_{0.1})P$ plotted in a semi-log scale. Shadowed areas mark Li(Mn), and vertical arrows mark the position where we measured $\frac{1}{T_1}$ of the Li(Mn) site. Note that the total spin echo intensity is not normalized, and the origin is shifted vertically for different temperatures for clarity.

SQUID in B_{ext} = 4 T (solid curve). Also presented in the inset is M measured in B_{ext} = 0.01 T, establishing the bulk ferromagnetism below T_c = 25 K. In general, $^7K = {}^7K_{spin} + {}^7K_{orb} = (A_0/g\mu_B)\chi_{spin} + {}^7K_{orb}$. The small orbital shift $^7K_{orb}$ is temperature independent ($\sim +0.05\%$ in the present case), while the hyperfine coupling between the Mn electron spins and the Li nuclear spin, $A_0 = -12$ kOe/μ_B, turns out to be negative for the Li(Mn) peak, hence the overall sign of $^7K < 0$. Note that $-^7K$ reaches as large as 3.5 %.

In contrast with the Li(Mn) sites, ^7K at Li(0) remains small and comparable to that in nonmagnetic LiZnP (see Fig. 1). The HHFW of Li(0), however, is much broader than that of LiZnP (∼5 KHz), and continuously increases from 20 KHz at 280 K to 240 KHz at 4.2 K. The fact that HHFW of Li(0) is an order of magnitude broader in $LiZn_{0.9}Mn_{0.1}P$ suggestss that the hyperfine magnetic fields from the doped Mn strongly affect *all* Li sites, including those without Mn atoms at n.n. Zn sites. Our findings in Fig. 3 are consistent with our μSR results observed for the same sample that the ferromagnetic volume fraction reaches 100 %[17].

To gain additional insight into the nature of Mn spins, we also measured the nuclear spin-lattice relaxation rate $\frac{1}{T_1}$ at the Li(0) peak and the center of the broad Li(Mn) peak, as marked by downward arrows in Fig. 2. We note that we do not observe satellite peaks corresponding to the $\pm\frac{1}{2}$ - $\pm\frac{3}{2}$ transitions for both Li(0) and Li(Mn) sites. This is not surprising, in view of the fact that even the Li(Mn) sites are still located in a high symmetry environment; Mn^{2+} ions are isovalent with Zn^{2+} ions, and the difference between the ionic radius of Mn^{2+} (0.083 nm) and that of Zn^{2+} (0.074 nm) is small. We also confirmed that the radio frequency pulse width optimized for the Li(Mn) and Li(0) peaks is identical with that of LiZnP, implying that the Li(0) peak does not arise from the $+\frac{1}{2}$ to $-\frac{1}{2}$ transition alone. If the sharper Li(0) peak in the middle originated only from the $+\frac{1}{2}$ to $-\frac{1}{2}$ transition, the pulse width should be narrower by a factor of 2. These findings indicate that we are observing a superposition of the $+\frac{1}{2}$ to $-\frac{1}{2}$ and $\pm\frac{1}{2}$ to $\pm\frac{3}{2}$ transitions in all cases, which would lead to a single exponential recovery curve for the spin-lattice relaxation process. Since our sample is an alloy-doped with Mn^{2+} magnetic moments, however, $\frac{1}{T_1}$ is bound to have a distribution. We therefore use a stretched exponential function to fit the T_1 recovery data in all cases (see Supplemental Materials)[22]. This is a standard practice for NMR studies of inherently disordered magnetic materials.

We summarize the results of $\frac{1}{T_1}$ in Fig. 4. The nuclear spin-lattice relaxation time T_1 represents the time scale during which Li nuclear spins relax to their thermal equilibrium after the absorption of radio frequency pulses. $\frac{1}{T_1}$ becomes larger when more low energy spin excitations associated with the Mn spins or the conduction electrons exist. Theoretically, the spin contribution to $\frac{1}{T_1}$ may be written using the imaginary part of the dynamical electron spin susceptibility $\chi''(\mathbf{q}, f_o)$ as $\frac{1}{T_1} \propto T\sum_{\mathbf{q}} |A(\mathbf{q})|^2 \frac{\chi''(\mathbf{q},f_o)}{f_o}$[23], where $A(\mathbf{q})$ is the hyperfine form factor[23]. In the parent compound LiZnP, $\frac{1}{T_1}$ of the Li(0) sites is as slow as $\sim 0.004\ s^{-1}$. Such very slow relaxation rates are typical for non-magnetic insula-

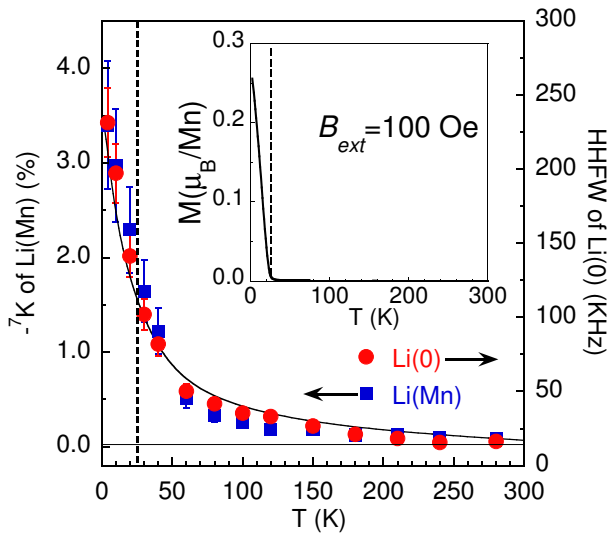

FIG. 3: (Color online) The temperature dependence of the ^{7}Li NMR Knight shifts, -^7K, at the Li(Mn) sites (■). The sign of ^7K is reversed, to take into account the negative sign of the hyperfine coupling A_o. The horizontal solid line represents $^7K_{orb}$ = 0.05%. Also shown is the HHFW of Li(0) in $Li(Zn_{0.9}Mn_{0.1})P$ (•). For comparison, we overlay the temperature dependence of the bulk *dc*-magnetization M at 4 Tesla measured with SQUID (solid curve, normalized at 4.2 K). Inset: the *dc*-magnetization M measured at B_{ext} = 100 Oe; M increases sharply below T_c = 25 K. Notice that this feature is suppressed at B_{ext} = 4 Tesla. Dashed lines mark T_c = 25 K.

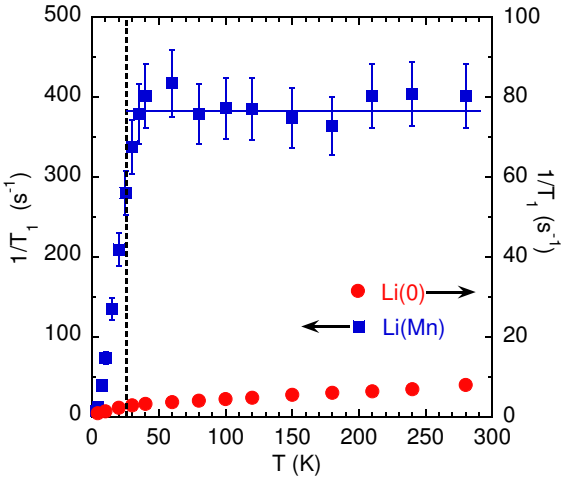

FIG. 4: (Color online) $\frac{1}{T_1}$ of Li(0)(•) and Li(Mn)(■) of $LiZn_{0.9}Mn_{0.1}P$, with the solid line as a guide for the eyes. The dashed line marks T_c = 25 K.

tors, and consistent with the fact that both Mn moments and conduction carriers are absent in the non-magnetic semiconductor LiZnP.

Upon Mn doping, the relaxation rate increases dramatically. $\frac{1}{T_1} \sim 400$ s^{-1} at the Li(Mn) site observed above T_c is five orders of magnitude enhanced compared with the non-magnetic LiZnP. This finding provides evidence for the presence of strong, low-frequency Mn spin fluctuations in the paramagnetic state above T_c. The suppression of $\frac{1}{T_1}$ below $\sim T_c$ indicates that these spin fluctuations are suppressed once ferromagnetic long-range order is established. The temperature independence of $\frac{1}{T_1}$ in the broad temperature range from 280 K down to $\sim$ 30 K also implies that the Mn spin-spin correlations are in the so-called exchange narrowed regime[24], where the energy scale of the thermal disturbance (k_BT) is comparable to or greater than that of the typical Mn-Mn spin interaction $|J|$. Using the Gaussian approximation for the spin-spin correlation function, we can express $\frac{1}{T_1} = \sqrt{2\pi}\frac{S(S+1)}{3\omega_e}(\frac{A_0}{\hbar})^2 \sim 400s^{-1}$[24], where $S \lesssim 5/2$[9] and $A_0 = -12$ kOe/μ_B as determined from Fig. 3. Therefore we estimate the characteristic frequency of the Mn spin fluctuations as $\omega_e \sim 1.1 \times 10^{15}$ rad/s in the paramagnetic state above T_c .

This large value of ω_e sets a strong constraint on the nature of Mn-Mn spin interactions. First, we recall that $\omega_e^2 = \frac{2}{3}zS(S+1)(\frac{J}{\hbar})^2$ within the Gaussian approximation[24], where z is the number of Mn sites within the range of Mn-Mn interactions. Since the high temperature regime with a constant $1/T_1 \sim 400$ sec^{-1} extends to $\sim T_c$, the typical Mn-Mn spin interaction energy scale $|J|$ is at most ~ 100 K. This implies that the number of Mn sites within the range of Mn-Mn interactions is as large as $z \sim 10^3$. While our estimation may be somewhat crude, our $1/T_1$ data establishes that each Mn spin interacts with a very large number of other Mn spins, rather than just a few Mn sites in the immediate vicinity. Our finding is consistent with the earlier theoretical proposal that the Mn-Mn spin interactions are caused primarily by the long-range interactions, such as the p-d Zener exchange interaction mediated by conduction carriers (doped holes or electrons)[25], which is the semiconductor analogue of the RKKY interaction in metals. We note, however, that our finding based on ω_e only implies the extended nature of the Mn-Mn interactions, and does not rule out other interaction mechanisms.

$\frac{1}{T_1}$ at the main Li(0) peak of $LiZn_{0.9}Mn_{0.1}P$ is slower than the Li(Mn) site by a factor of ~ 50. This is consistent with the fact that Li(0) sites do not have Mn at their n. n. sites, hence the effects of Mn spin fluctuations are much more limited due to weaker hyperfine couplings. Nonetheless, $\frac{1}{T_1}$ at the Li(0) peak also exhibits a kink around T_c, indicating that Li(0) sites are indeed under the influence of ferromagnetic Mn spin fluctuations as well. The observed linear increase of $\frac{1}{T_1} \sim a+bT$ above T_c suggests that Li(0) nuclear spins may have two separate relaxation mechanisms. The constant a-term is caused by Mn spin fluctuations, in analogy with the constant behavior observed for Li(Mn), while the small T-linear bT-term may be attributed to the Korringa process[21] arising from the Fermi surface excitations of a small number of conduction carriers. These carriers might also facilitate the interactions between distant Mn sites.

To summarize, the successful synthesis of the bulk form of I-II-V DMS, $LiZn_{0.9}Mn_{0.1}P$ with $T_c = 25$ K, enabled us to investigate the nature of its ferromagnetism by microscopic ^{7}Li NMR techniques. In particular, by successfully identifying the ^{7}Li NMR signals arising from the Li sites n. n. to the Mn spins, we were able to probe the static and dynamic magnetic susceptibility of Mn spins through the NMR Knight shift and $1/T_1$. We deduced the characteristic Mn spin fluctuation frequency ω_e, and showed that the Mn-Mn spin interaction extends many unit cells. Regardless of the exact mechanism of such interactions, our findings explain why DMS could exhibit a relatively high T_c with a low density of Mn.

The work at Zhejiang University was supported by National Basic Research Program of China (No.2011CBA00103), NSF of China (No.11274268), Zhejiang Provincial Natural Science Foundation of China (LY12A04006) and Fundamental Research Funds for Central Universities (2013QNA3016). The work at McMaster was supported by NSERC and CIFAR. F.L. Ning acknowledges helpful discussions with Y.J. Uemura, C.Q. Jin, F.C. Zhang, X. Wan and C. Cao.

* Electronic address: ningfl@zju.edu.cn

1. H. Ohno, A. Shen, F. Matsukura, A. Oiwa, A. Endo, S. Katsumoto, and Y. Iye, Appl. Phys. Lett. **69**, 363 (1996).
2. A.H. MacDonald, P. Schiffer, andN. Samarth, Nature Materials **4**, 195 (2005).
3. T. Jungwirth, J. Sinova, J. Masek, J. Kucera, and A. H. MacDonald, Rev. Mod. Phys. **78**, 809 (2006).
4. T. Dietl, Nature Materials **9**, 965 (2010).
5. M. Wang, R.P. Campion, A.W. Rushforth, K.W. Edmonds, C.T. Foxon, and B.L. Gallagher, Appl. Phys. Lett. **93**, 132103 (2008).
6. I. Zutic, J. Fabian, and S. Das Sarma, Rev. Mod. Phys. **76**, 323 (2004).
7. N. Samarth, Nature Materials **9**, 955 (2010).
8. S. Chambers, Nature Materials **9**, 956 (2010).
9. Z. Deng, C.Q. Jin, Q.Q. Liu, X.C. Wang, J.L. Zhu, S.M. Feng, L.C. Chen, R.C. Yu, C. Arguello, T. Goko, F.L. Ning, J.S. Zhang, Y.Y. Wang, A.A. Aczel, T. Munsie, T.J. Williams, G.M. Luke, T. Kakeshita, S. Uchida, W. Higemoto, T.U. Ito, B. Gu, S. Maekawa, G.D. Morris, and Y.J. Uemura, Nature Communications **2**, 422 (2011).

[10] J.K. Furdyna, J. Appl. Phys. **64**, R29-R64 (1988).
[11] P.M. Shand, A.D. Christianson, T.M. Pekarek, L.S. Martinson, J.W. Schweitzer, I. Miotkowski, and B.C. Crooker, Phys. Rev. B **58**, 12876 (1998).
[12] R. Bacewicz, and T.F. Ciszek, Appl. Phys. Lett. **52**, 1150 (1988).
[13] K. Kuriyama, and F. Nakamura, Phys. Rev. B **36**, 4439 (1987).
[14] K. Kuriyama, T. Kato, and K. Kawada, Phys. Rev. B **49**, 11452 (1994).
[15] S.H. Wei, and A. Zunger, Phys. Rev. Lett. **56**, 528 (1986).
[16] S.R. Dunsiger, J.P. Carlo, T. Goko, G. Nieuwenhuys, T. Prokscha, A. Suter, E. Morenzoni, D. Chiba, Y. Nishitani, T. Tanikawa, F. Matsukura, H. Ohno, J. Ohe, S. Maekawa, and Y.J. Uemura, Nature Materials **9**, 299 (2010).
[17] Z. Deng, F.L. Ning, Y.J. Uemura, C.Q Jin et al., Submitted to Phys. Rev. B.
[18] K. Kuriyama, T. Katoh, and N. Mineo, Journal of Crystal Growth **108**, 37 (1991).
[19] J.B. Boyce, and C.P. Slichter, Phys. Rev. Lett. **32**, 61 (1974).
[20] J. Bobroff, W.A. MacFarlane, H. Alloul, P. Mendels, N. Blanchard, G. Collin, and J.-F. Marucco, Phys. Rev. Lett. **83**, 4381 (1999).
[21] C.P. Slichter, *Principles of Magnetic Resonance* (Springa-Verlag, Berlin, 1990).
[22] See Supplemental Material at [URL] for the measurement procedures.
[23] T. Moriya, J. Phys. Soc. Jpn. **18**, 516 (1963).
[24] T. Moriya, Prog. Theor. Phys. **16**, 641 (1956).
[25] T. Dietl, Science **287**, 1019 (2000).